GPR surveys for the characterization of foundation plinths within a seismic vulnerability analysis

2013 J. Geophys. Eng. 10 034007

(http://iopscience.iop.org/1742-2140/10/3/034007)

IOP Publishing Journal of Geophysics and Engineering
J. Geophys. Eng. **10** (2013) 034007 (9pp) doi:10.1088/1742-2132/10/3/034007

GPR surveys for the characterization of foundation plinths within a seismic vulnerability analysis

Domenica De Domenico, Antonio Teramo and Davide Campo

Seismological Observatory, University of Messina, via Osservatorio 4, I-98121 Messina Italy

E-mail: dedomenicod@unime.it

Received 31 October 2012
Accepted for publication 4 April 2013
Published 5 June 2013
Online at stacks.iop.org/JGE/10/034007

Abstract
We present the results of GPR surveys performed to identify the foundation plinths of 12 buildings of a school, whose presence is uncertain since the structural drawings were not available. Their effective characterization is an essential element within a study aimed at assessing the seismic vulnerability of the buildings, which are non-seismically designed structures, located in an area classified as a seismic zone after their construction. Through GPR profiles acquired by two 250 MHz antennas, both in reflection mode and in a WARR configuration, the actual geometry and depth of the building plinths were successfully identified, limiting the number of invasive tests necessary to validate the GPR data interpretation, thus enabling the choice of the most suitable sites that would not alter the serviceability of the structure. The collected data were also critically analysed with reference to local environmental noise that, if causing reflections superimposed on those of the subsoil, could undermine the success of the investigation. Due to the homogeneity of the ground, the processing and results relative to each pair of profiles carried out for all of these buildings is very similar, so the results concerning only two of them are reported.

Keywords: GPR, foundation plinth, WARR, building seismic vulnerability, non-destructive test

(Some figures may appear in colour only in the online journal)

1. Introduction

The characterization of the actual geometry of the foundation structures constitutes one of the most important and interesting elements in the buildings' seismic vulnerability assessment, in order to determine the collapse mechanisms, also in reference to the level of prefigurable constraint between the structures of elevation and foundation. This requirement takes on greater significance when the examined buildings, built in the absence of a specific seismic code, must meet the requirements of current seismic Italian standards (NTC 2008).

The buildings on which the surveys were performed are located in a school in Piazza Armerina (Enna, Italy). This town was not officially recognized as a seismic zone at the time of the structures' construction (1962).

The approach for a fair and effective use of GPR investigations in the field of structural diagnostics moves on from the requirements of the Italian seismic rules. These rules involve the acquisition of a certain level of knowledge in relation to the type and the extent of documentation to be acquired for the geometric and structural characterization of the studied buildings. The non-invasiveness and reliability of the GPR surveys make this technique particularly suitable for structural diagnostics. It is widely used with success in this sector, also in relation to the speed of data collection and its immediate display. The latter allows a prompt reading of the subsoil situation and the verification of the setting for the effectiveness of measurement setting at the same time (Annan 2002, Arndt and Jalinoos 2009, Hugenschmidt and Loser 2007, McCann and Forde 2001, Binda *et al* 2003).

GPR surveying has been a technique widely used in geological settings and civil engineering applications since the early 1980s (Grandjean *et al* 2000); it can be used to obtain information about several features such as layer thickness (Loizos and Plati 2007, Al-Qadi and Lahouar 2005), the location of reinforcing bars and metal elements in concrete bases or structures (Barrile and Pucinotti 2005, Shaw *et al* 2005, Hugenschmidt and Mastrangelo 2006, Bottari *et al* 2003, De Domenico *et al* 2013) and to check the depth of damage observed on the surface (Pérez-Gracia 2008b). A useful review of GPR applications in concrete can be found in Bungey (2004).

In this paper we deal with GPR surveys performed in order to get information about the presence of foundation plinths, and their characterization through their relative shape and depth. In this work, owing to the homogeneity of the ground and the similar processing and results in proportion to their different structural characteristics, data relating to only two reinforced concrete buildings are shown. The first case will be discussed in greater detail, due to the complexity of its study. Indeed, the local environmental noise, causing reflections superimposed on those of the subsoil, could undermine the success of the investigation. Having properly recognized and eliminated the cause of the noise, thanks to the GPR WARR acquisition mode, the actual geometry and depth of the building plinths are successfully identified all the same, limiting the invasive tests necessary to validate GPR data interpretation.

2. Preliminary considerations about the GPR survey

Knowledge of the horizontal resolution and penetration depth are essential for the design and operation of the GPR survey (Jol 2010). They are determined by antenna frequency and the electrical properties of the subsoil (Olhoeft 1998, Daniels 2004).

These considerations are preliminary and are even more important for the success of the detection of the plinths. In this specific case the dimensions and the depth of the plinths were not known *a priori* because of the lack of structural drawings, and could vary widely from building to building, so we can just hypothesize them. The only data on which the assumptions can be based are the structural elements, visible and measurable externally, correlated to those of the foundations.

The studies of the two school buildings reported in this paper as illustrative cases were the most significant, because they represent the extreme cases with regard to the size and depth of the foundations and therefore the horizontal resolution too. The former was the most imposing and highest building (12 m), while the second was among the lowest (6 m) for which excavations were realized. The first building stood on a rectangular surface wider than 500 sq m (17 m $\times$ 33 m) and consists of a reinforced concrete single span frame. Given its height, the foundations depth should be greater than 2 m while, assuming the base section as a square and no less than three times greater than the column section (0.25 m^2), the plinth side should have a length not less than 1.5 m. In the second building the foundation plinth is less deep than the first one and its side length must measure not less than 0.9 m, as the column side is equal to 0.3 m.

Considering these preliminary hypotheses, the theoretical horizontal resolutions necessary to distinguish the structural details of the foundations at various depths were calculated for different values of dielectric permittivity characteristics of the soil of the investigated site and different central frequencies of the potentially exploitable antennas that could be used.

In general, the horizontal resolution Δ_H, or spatial resolution, is defined as the ability to distinguish two close elements, at the same depths, as two different anomalies (Daniels *et al* 1988); it depends on the characteristics of the radar signal (antenna central frequency), the survey (trace interval), the electromagnetic properties of the medium that affect the radiation pattern and the distance from the antenna to the target. In other words it is assumed that the horizontal resolution depends on the size of the antenna footprint, estimated as the first Fresnel zone (Pérez-Gracia *et al* 2008a).

This zone of influence is defined as the area which can contain a second target that cannot be uniquely resolved. Its diameter d is calculated by many authors (Huisman *et al* 2003, Pérez-Gracia 2001) with the following relationship:

$$d = \Delta_H = \sqrt{\frac{\lambda^2}{4} + z\lambda} \tag{1}$$

where z is the depth and λ is the wavelength calculated at the nominal frequency of the antenna.

The electromagnetic characteristics of the soil were assumed to be homogeneous throughout the volume investigated, neglecting any variations due to the thin surface layer of asphalt. The soil, consisted of silty sands, was considered not saturated at the explored depth. This was very probable, in relation to the environmental conditions it was operated in for which values of relative electric permittivity, ε_r, between 3 and 5 are reported in the literature (Reppert *et al* 2000). Only these two values were used for the horizontal resolution calculation, ignoring a possible rise in permittivity due to the percentage of silt present (>12%), which having an adsorbent power greater than the sand, can more easily retain water which may exert a strong control on the dielectric properties of geological materials, as described in Davis and Annan (2006).

The values of the electromagnetic waves' propagation velocity were calculated using the simplified relation (2) valid for low loss media (Sharma 1997), as for frequencies above 100 MHz the independence of it from the frequency of the electromagnetic signal was demonstrated (Reppert *et al* 2000), where c is the speed of light in vacuum, $c = 3 \times 10^8$ m s^{-1}.

$$v = \frac{c}{\sqrt{\varepsilon_r}} \tag{2}$$

These calculated values are equal to 0.173 and 0.134 m ns^{-1} for $\varepsilon_{r1} = 3$ e $\varepsilon_{r2} = 5$ respectively, and allow us to deduce the value of λ required for the determination of the theoretical horizontal resolution Δ_H that is calculated via the relation (1) with depth steps of 50 cm up to a maximum of 6 m, at three different frequencies of the potentially utilizable antennas for the investigation, 100, 250 and 500 MHz, as shown in table 1.

The best resolution was obtained with the highest frequency, 500 MHz, but, given the conditions of the soil

Table 1. Theoretical horizontal resolution calculated up to maximum depth of 6 m, with a step of 50 cm, for the values $\varepsilon_{r1} = 3$ and $\varepsilon_{r2} = 5$ and their respective velocities, at the frequencies of 100, 250 and 500 MHz.

	Horizontal resolution Δ_H (m)					
	$\varepsilon_{r1} = 3$, $v_1 = 0.173$ m ns^{-1}			$\varepsilon_{r2} = 5$, $v_2 = 0.134$ m ns^{-1}		
Depth z (m)	100 MHz	250 MHz	500 MHz	100 MHz	250 MHz	500 MHz
0.50	0.93	0.59	0.42	0.82	0.52	0.36
1.00	1.31	0.83	0.59	1.16	0.73	0.52
1.50	1.61	1.02	0.72	1.42	0.90	0.63
2.00	1.86	1.18	0.83	1.64	1.03	0.73
2.50	2.08	1.32	0.93	1.83	1.16	0.82
3.00	2.28	1.44	1.02	2.01	1.27	0.90
3.50	2.46	1.56	1.10	2.16	1.37	0.97
4.00	2.63	1.66	1.18	2.31	1.46	1.03
4.50	2.79	1.76	1.25	2.45	1.55	1.01
5.00	2.94	1.86	1.32	2.59	1.64	1.16
5.50	3.08	1.95	1.38	2.71	1.72	1.21
6.00	3.22	2.04	1.44	2.84	1.79	1.27

under examination, the penetration depth of the signal at this frequency may be insufficient for the prefigured goal; on the other hand the use of an antenna with a frequency of 100 MHz, because of its poor resolving power (approximately 2 m at a depth of 2.5 m), could lead to significant complexity in the discrimination of the reflections of the plinths. As regards the frequency of 250 MHz, Δ_H was maintained lower than required: from 1.5 m up to 3.5 m in depth in the case of low permittivity, and up to 4.5 m in the case of high permittivity. In this way, this frequency presented acceptable values of resolution at the presumed depth, and having an attenuation coefficient half of that at 500 MHz, resulted in a far superior degree of penetration.

However, the required resolution and penetration depth were quite different in both cases. For the above-mentioned reasons, the use of a system with GPR antennas at a frequency of 250 MHz appeared to be the best compromise between horizontal resolution and depth of penetration, within which it is assumed you can track the foundation plinths if they are really present, bearing in mind that the second building case was a borderline case.

The use of this table proved to be practical and appropriate mainly for two reasons. Firstly, it immediately enabled us to choose, on a case-by-case basis, the most suitable frequency of antenna to resolve anomalies presumably ascribable to plinths different in depth, size, structural features, and the design of the various buildings, also in their turn, of heterogeneous height, size and intended use. Secondly, it was possible to verify if the frequency used was adequate for those determined structures brought to light by the excavation. Afterwards the drawings relating to the exact geometry of the plinths were planned, making comparison possible with what was deduced from the radargrams.

3. The GPR surveys

3.1. Acquisition and processing for GPR surveys

In both cases, the GPR surveys were performed only outside the buildings because the partition walls did not allow us to make the acquisitions inside it, using a GPR system produced by Mala Geoscience equipped with two shielded antenna with nominal central frequency of 250 MHz.

A first profile was carried out in reflection mode (common-offset survey), to obtain an 'image' of the subsoil: a scan was acquired along a side of the building, keeping the antenna adjacent to it, adding a margin of 2 m beyond the two ends of the same. On the same acquisition line, but in an intermediate part of it, a second profile was performed with the WARR (wide angle reflection and refraction) method, to estimate the EM signal velocity distribution as well as the depths of the reflecting interfaces, using two separate antennas with the same central frequency and maintaining the transmitter in a fixed position (common-source survey) while the receiver antenna was gradually moved away. Figure 1 shows the profile map relative to the first building; in the second case only the length of the building was different. The co-polarized parallel dipole configuration was chosen because it gives the widest angular coverage of a subsurface reflector. For both surveys, the sample frequency was set to about 2.3 GHz and the adopted trace interval was 5 cm, the smallest value allowed by the georadar equipment using this antenna. This value was consistent with the required resolution and allowed us to scan the greatest possible number of traces, particularly necessary in the common-source survey, in order to obtain the most defined velocity spectrum for this specific context.

The two acquisitions were analysed, with their processing carried out using the software Reflexw (Sandmeier 2011), starting from the common source data analysis, because the results of these were preliminary for the development of common offset data processing: the migration and the time-depth conversion of the radargram were performed by means of the velocity model obtained from 1D WARR.

3.1.1. Common source data analysis. The WARR data were processed with automatic gain control to make the weaker reflections visible, and band pass filtering to increase the S/N ratio. The profile discussed here in greater detail is relative to the first building (figure 2(*a*)), because the processing of the

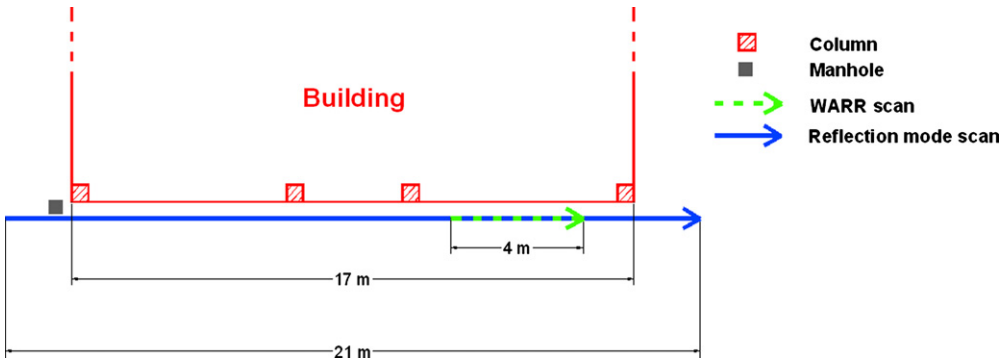

Figure 1. GPR scan lines position: the WARR was performed between the third and fourth column to avoid the plinths' reflections. Both the surveys were performed at a distance of about 50 cm from the perimetral wall of the first building.

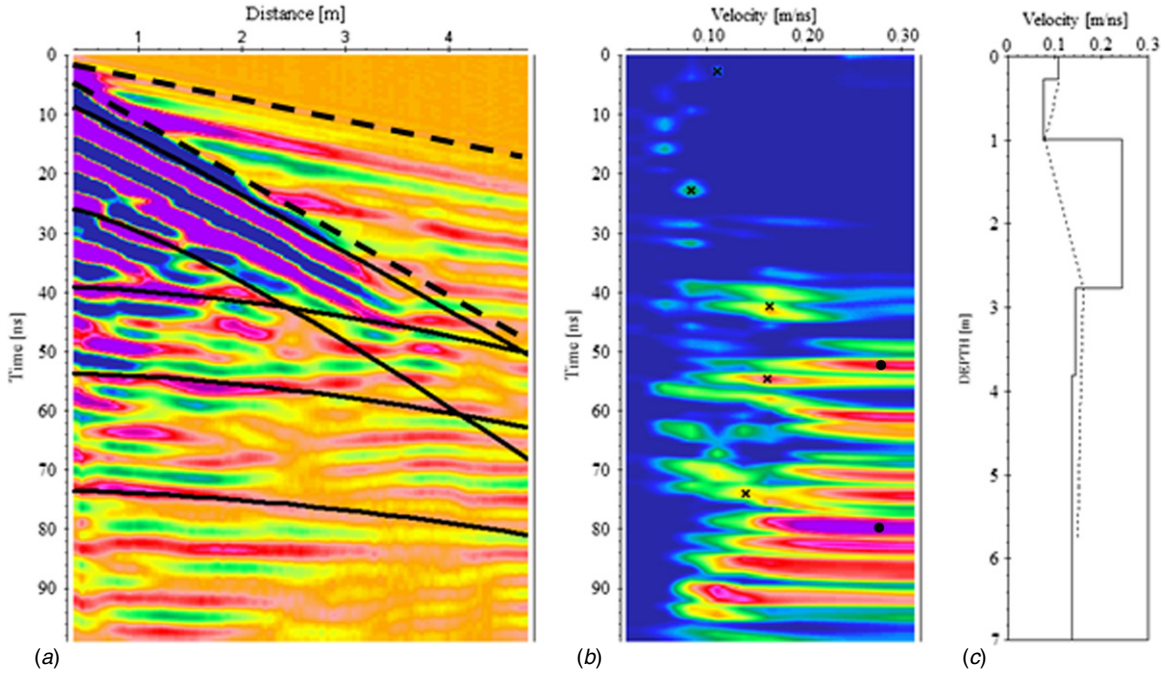

Figure 2. (*a*) The WARR profile with the immediate visualization of the hyperbolic ground reflections (black lines), the air and the ground direct waves (dashed lines); (*b*) the velocity/time spectrum calculated through the semblance analysis: the *x* symbols define the velocities calculated for the picked reflections, the black spots refer to the reflections in air and their multiples shown in (*a*); (*c*) the one-dimensional velocity distribution together with the VRMS-distribution (dashed line).

other profiles was along the same in broad lines. Conversely, this case presented a particular problem which made it the most complicated study in respect to the others, as will be seen.

In this processed profile the direct waves in the air and in the ground were distinguished by their characteristic linear progression starting from the origin (dashed lines in figure 2(*a*)) and the reflections related to buried interfaces showing the typical hyperbolic trend existing between the travel time and the antennas (black continue lines in figure 2(*a*)) offset (Salih 2006, Bohidar and Hermance 2002).

Then semblance analysis was employed. This technique allows a velocity-depth distribution in the subsoil to be obtained, locating the maximum energy points in the velocity/time spectrum (Yilmaz 1987, Dix 1955, Taner and Koehler 1969): the root mean square velocity (v_{rms}) is used for calculating the reflection hyperbola and for determining the layer velocities by the semblance analysis.

The velocity spectrum thus obtained (figure 2(*b*)) highlights the different peaks with their multiples associated with the different layers of the subsoil, (***x*** symbols), but, above all, also highlights peaks corresponding to velocity values of about 0.28 m ns^{-1} (black spots), that were miscounted in the velocity model building because they are related to objects on or above the acquisition plane, as suggested in Sun and Young 1995. In fact, the high dispersion of the electromagnetic beam in air, its lossless nature (Conyers and Goodman 1997, Rial *et al* 2009) and the imperfect shielding of the antenna, due to the size of the low frequency dipoles (which was difficult to shield maintaining, at the same time, a reasonable size for the whole GPR system (Van der Kruk

and Slob 2004)), can determine an unwanted reception of signals reflected by objects located above the scan plane, even if apparently far from the acquisition line. These reflections appear superimposed on those produced by the objects actually present in the subsoil; therefore recognizing these signals is fundamental to avoid misinterpretation.

In this case, the cause of the above-surface reflections was identified in the peculiar shape of the building equipped with a metal roof covering, whose distance from the scan line was equivalent to that obtainable from the corresponding two-way travel times in the air. Nevertheless, the velocity model (figure 2(*c*)), built with the pick series referable to the subsoil, indicated by ***x*** symbols in figure 2(*b*), showed an initial increase of speed followed by a progressive decrease with depth. The EM wave velocity generally decreases with depth (Sun and Young 1995), a condition that was not verified in this case, maybe due to their artificial nature, as will be seen in detail when we analyse the reflection mode profile.

3.1.2. Common offset data analysis. During acquisition, some markers, shown in the upper part of radargram, were used to indicate the column position of the building, and are denoted by A, B, C and D where the presence of the plinths was strongly suggested. Furthermore, in the profile related to the first building, indicated in figure 3, the first pair of markers, denoted by M, identified the location of a metal manhole cover.

The common offset data had a time zero correction dc filtering applied to eliminate the time constant shift, a divergence compensation algorithm which allowed us to compensate for geometrical divergence losses, and, finally, Butterworth band-pass filtering was applied with the lower and upper frequency cut-off of 70 and 390 MHz respectively.

Concerning the first building, its radargram (figure 3(*a*)) showed three horizontally coherent reflections along the whole profile, temporally consistent between: 0 and 20 ns, 30 and 45 ns and over the 55 ns. At about 50 ns four couples of anomalies were detectable, corresponding to the markers A, B, C and D at the edges of each column, shown through ellipses. To better distinguish between these anomalies, the background removal filter was applied up to 47 ns and finally, the diffraction migration and the time-depth conversion were performed using the velocity model obtained from WARR data analysis (figure 3(*b*)). These settings provided a better visualization of the aforementioned anomalies, presumably due to the reflections from the plinths.

The migration is one of the most important filters: because a section often does not represent the 'true' position of the reflectors, mainly for steep layers, if strong diffractions are present, the migration tries to contract these diffractions to a minimum, giving a better approximation to the reality, which is useful for the successive interpretation.

The profile relative to the second building was processed in the same way and the resulting radargram is shown in figure 5(*a*), where the anomalies probably related to the plinths were well sketched. The corresponding 1D velocity model, used for the migration algorithm and the time-depth conversion, was obtained through another WARR, left out for brevity, since it does not present particular interpretation problems.

3.2. Results interpretation

As regards the first building, cross-analysis of the GPR data in reflection mode and WARR allowed the following significant anomalies and layers to be located and identified (figures 3(*a*) and (*b*)), mainly for the recognition of the reflections due to elements external to the subsoil investigated.

1. In the first 8 ns, the asphalt layer was about 30 cm thick, characterized by a velocity 0.11 m ns^{-1} and $\varepsilon_r = 7.43$;
2. Between 8 and 20 ns (0.30–1m deep) several reflections were noticeable due to an irregular distribution of pebbles with v = 0.08 m ns^{-1} and $\varepsilon_r = 14$; over a zone where a signal attenuation referable to a filling material was detectable;
3. Between 30 and 45 ns, an extended horizontal reflection was highlighted (figure 3(*a*)), along the whole profile already identified by the above mentioned WARR analysis, referable to the metal roof of the building located corresponding to the acquisition line. Such a hypothesis was confirmed by the decrease of the amplitude reflection over the aforementioned coverage, as well as a two-way travel time of 35 ns, corresponding to a distance of about 10 m, calculated with the velocity value of the EM waves in the air, equal to twice the space between the metal roof and the paving where the acquisition was made. This justifies the increase of velocity between 1 and 3 m shown in figure 2(*a*). This is also observable in figure 2(*c*), since the 40 ns hyperbola intercepts the direct ground wave and the first layer hyperbola, whose asymptote is the same ground wave. After the elimination of this horizontal band in figure 3(*b*), a more attenuated layer due to filling material was noticeable up to about 40 ns indicated with the grey line.
4. Over 42 ns (3–4 m deep), again a sharp increase of the reflection amplitude was evident. In particular, some oblique reflections were detected, indicated by the continuous segments in figure 3(*b*), corresponding to the edges of the plinths, under the individual columns whose position was indicated by the letters A, B, C and D, on the axis of the distances. This was due to a sharp contrast between the relative dielectric permittivity of different materials present in this layer: the concrete of the plinths and of the backfill surrounding sandy material that covers them. The left reflection was not defined at the A marker, where the geometry of the plinth of the first column was not wholly identifiable as that of the others, being affected by the reflection of the metal manhole placed at the level of the paving (denoted M). This layer corresponded to the foundation terrain with a mean value of v = 0.14 m ns^{-1} and $\varepsilon_r = 4.59$; the location and the shape of the anomalies were consistent with those typical of foundation plinths of the column. In particular, figure 3(*c*) reproduced the foundation plinths' shape very closely to their actual geometry, as revealed and drawn (figure 4(*b*)) after excavation (figure 4(*a*)). It was easy to see the very great similarity to the anomalies highlighted in figure 3(*b*); in this case the grey line corresponds to the top of the plinths.

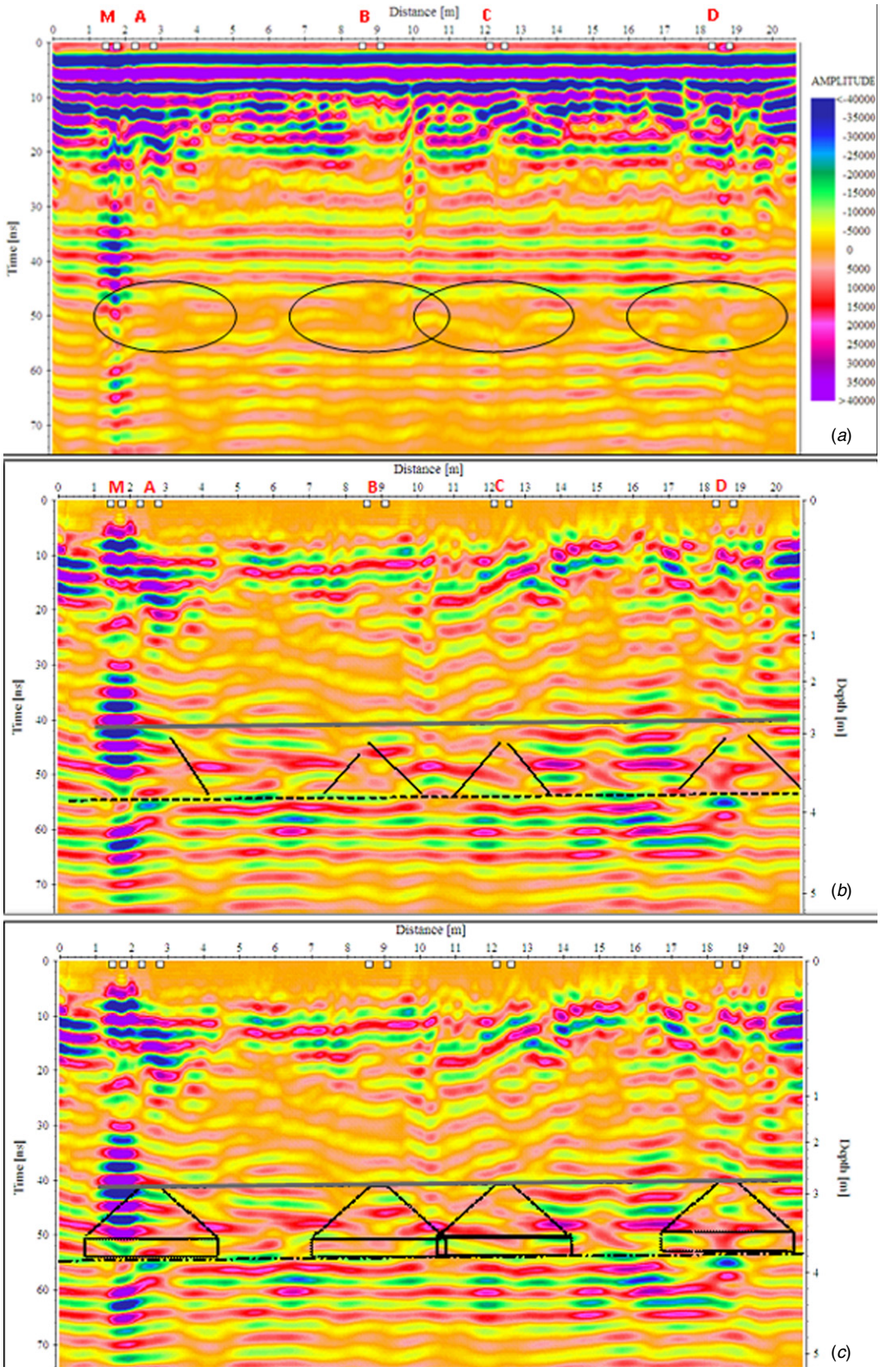

Figure 3. Reflection scan mode related to the first building. The markers A, B, C and D indicate the columns' position while M denotes a metal manhole. (*a*) Standard processed section, the ellipses highlight the anomalies found on the sides of each column. (*b*) Migrated section with background removal filter up to 47 ns; the continuous segments show some oblique reflections, in correspondence with the edges of the plinths; the grey line at 42 ns indicates the end of the backfill layer, the dashed line highlights the horizontal reflection probably due to the base of the plinths. (*c*) The foundation plinths' shape is sketched very close to the actual geometry as measured after the excavation. The grey line at 42 ns corresponds with the top of the plinths and the dashed line at 55 ns highlights the depth of the plinths base, the oversite concrete, corresponding to a depth of about 3.8 m.

(*a*)

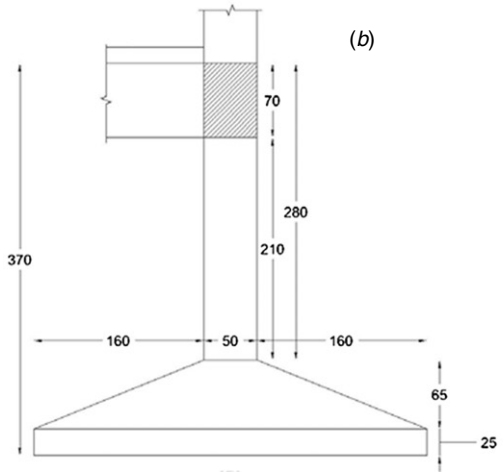

Figure 4. (*a*) Two snapshots of the destructive test performed to validate the GPR data interpretation for the first building; (*b*) the actual geometry and depth of the dug up building plinths. The unit dimension is cm.

5. At 55 ns (about 4 m depth), another horizontal interface was highlighted, which allowed the depth of the plinths' base to stand out. The maximum depth level of the base of the foundation plinths was easily detectable. It was the oversite concrete, shown in figure 3(*b*) by the dashed line, via the more or less continuous horizontal interface reflection,, corresponding to a depth of about 3.8 m, consistent with findings from the excavation shown in figure 4.
6. What cannot be detected, because it was small compared to the resolution of the used antenna, was the width of the pillar equal to 50 cm.

The value $\varepsilon_r = 4.59$ calculated corresponding to the foundation terrain, agreed very well with the estimated values used for the calculation of the resolution discussed above, remaining within the range theoretically assumed. Therefore, it can be deduced that the used backfill was constituted by the same geologic material of the foundation soil, i.e. the silty sands, and that the percentage of silt was not likely to substantially change the permittivity of the sands.

For a rigorous calculation, invasive tests are necessary to validate GPR data interpretation, but in this case, the details of the obtained information allowed us to limit the numbers of destructive tests, thus being able to choose the most suitable site to not affect the serviceability of the structure. The destructive test corresponding to the analysed radar profile was shown in figure 4(*a*). It confirmed what was inferred from the GPR data and their processing, hence allowed us to successfully identify the actual geometry and depth of the building plinths and provide an accurate measured drawing, shown in figure 4(*b*).

The successive tests on the other building allowed us to detect the presence of the foundation plinths for this structure, highlighting their different depths and sizes of the base, as reported in figure 5(*a*). In fact, in this radar profile corresponding to the markers placed where the building columns lie, some vertical discontinuities created by pillars were visible up to not more than 80 cm deep, obviously given the small size of the column and the resolution of the used antenna. In the direction of the latter, at a depth of between 1.4 and 1.7 m, oblique discontinuities of the reflected signal were made out, indicated by oblique lines which revealed the presence of the foundations. The dotted line around the 1.8 m depth indicates the oversite concrete, that is the basis on which the plinths rest. Also in this case, an increase in the reflection amplitude in the central area between two adjacent columns was observed. This was caused by the convergence of the reflections generated on the interface between the two materials, the concrete of the columns and footings and the backfill, which presented a sharp contrast of dielectric permittivity. Even if the horizontal resolution based on the initial hypotheses was in a borderline case, the success of the survey was supported by evidence of other elements of the plinth: the column up to 80 cm and its base well highlighted in figure 5(*a*). All depths and dimensions of the identified elements in the radargram were consistent with the actual geometry of the plinth shown in figure 5(*b*), as measured after the destructive test conducted in this zone.

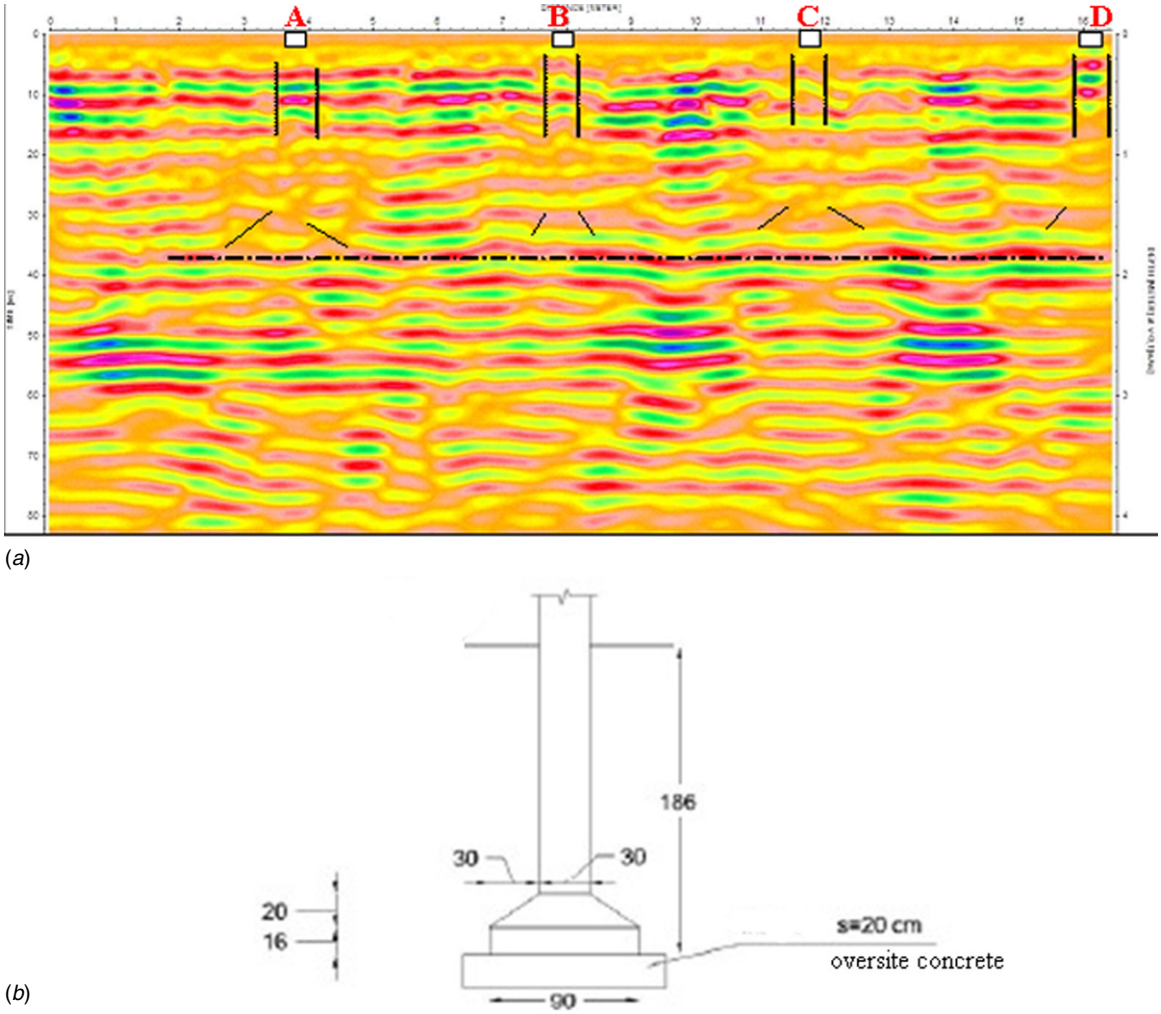

Figure 5. (*a*) Reflection scan mode profile of a standard processed section related to the second building. The markers A, B, C and D indicate the columns' position. In correspondence therewith the vertical discontinuities were underlined up to 80 cm deep; below them at a depth between 1.4 and 1.7 m the little oblique discontinuities revealed the probable presence of the foundations, indicated by oblique lines. The dotted line around the 1.8 m depth indicates the oversite concrete. (*b*) The actual geometry and depth of the building plinths as measured after the destructive test conducted in this zone. The unit dimension is cm.

4. Conclusions

The employment of a GPR system to detect the geometry and depth of the building foundation plinths, initially hypothesized, has shown high reliability and execution quickness. These are very important aspects and of not minor interest, since similar analysis had to be performed in 12 buildings extended over an area several hectares wide.

This enabled us to acquire specific evaluation elements within a study aimed at assessing the seismic vulnerability of the building itself, that is a non-seismically designed structure and located in an area that was classified as seismic zone after its construction.

The WARR data processing allowed us to build the 1D velocity model in order to reconstruct the possible site stratigraphy and to locate the foundation depth, as well in the particular analysed case to recognize the above-surface reflector (i.e. the metallic roof of the building), enabling its identification and the successive elimination, in the reflection mode data, in which otherwise it would have been interpreted as an additional layer in the subsoil. The eventual employing of an fk-filter to eliminate the direct airwave in the WARR data would also have eliminated these additional reflections, but in doing so they would not be recognized in the common offset data, thus leading to inevitable interpretation errors.

Moreover, it is important to underline, according to design codes, the proper complementary relationship of this investigation technique, as non-invasive surveys, with the destructive testing which must be carefully planned in order to achieve the required level of structural knowledge.

References

Al-Qadi I L and Lahouar S 2005 Measuring layer thicknesses with GPR—theory to practice *Constr. Build. Mater.* **19** 763–72

Annan A P 2002 GPR—history, trends and future developments *Subsurface Sensing. Technologies. and Applications.* vol 3 253–70

Arndt R and Jalinoos F 2009 NDE for corrosion detection in reinforced concrete structures: A benchmark approach *Proc. Non-Destructive Testing in Civil Engineering (Nantes, France, 30th June–3rd July)* www.ndt.net/article/ndtce2009/papers/171.pdf

Barrile V and Pucinotti R 2005 Application of radar technology to reinforced concrete structures: a case study *NDT&E Int.* **38** 596–604

Binda L, Lualdi M, Saisi A, Zanzi L, Gianinetto M and Roche G 2003 NDT applied to diagnosis of historic buildings: a case history *Proc. 3-Day Int. Conf. on Structural Faults and Repair (London, 1–3 July)* p 10

Bohidar R N and Hermance J F 2002 The GPR refraction method *Geophysics* **67** 1474–85

Bottari A, De Domenico D, Giannino F, Marino A and Teramo A 2003 On a GPR survey to characterize the structural configuration of a masonry building *Proc. 3rd Int. Conf. on NDT (Chania, Crete, Greece, 15–18 October)* pp 99–103

Bungey J H 2004 Sub-surface radar testing of concrete: a review *Const. Building Mat.* **18** 1–8

Conyers L B and Goodman D 1997 Ground-penetrating radar *An Introduction for Archaeologists* (Walnut Creek, CA: Altamira Press)

Daniels D J 2004 *Ground-Penetrating Radar* 2nd edn (London: The Institution of Electrical Engineers) chapters 2, 4

Daniels D J, Gunton D J and Scott H F 1988 Introduction to subsurface radar *Radar Signal Process.* **135** 278–320

Davis J L and Annan A P 1989 Ground penetrating radar for high resolution mapping of soil and rock stratigraphy *Geophys. Prospect.* **37** 531–51

De Domenico D *et al* 2013 FDTD modelling in high resolution 2D and 3D GPR surveys on a reinforced concrete column in a double wall of hollow bricks *Near Surf. Geophys.* **11** 29–40

Dix C H 1955 Seismic velocity from surface measurements *Geophysics* **20** 68–86

Grandjean G, Gourry J C and Bitri A 2000 Evaluation of GPR techniques for civil-engineering applications: study on a test site *J. Appl. Geophys.* **45** 141–56

Hugenschmidt J and Loser R 2008 Detection of chlorides and moisture in concrete structures with ground penetrating radar *Mater. Struct.* **41** 785–92

Hugenschmidt J and Mastrangelo R 2006 GPR inspection of concrete bridges *Cem. Concr. Compos.* **28** 384–92

Huisman J A, Hubbard S S, Redman J D and Annan A P 2003 Measuring soil water content with ground penetrating radar: a review *Vadose Zone J.* **2** 476–91

Jol H M 2010 *Ground Penetrating Radar: Theory and Applications* (Amsterdam: Elsevier)

Loizos A and Plati C 2007 Accuracy of pavement thickness estimation using different ground penetrating radar analysis approaches *NDT&E Int.* **40** 147–57

McCann D M and Forde M C 2001 Review of NDT methods in the assessment of concrete and masonry structure *NDT&E Int.* **34** 71–84

Olhoeft G R 1998 Electrical, magnetic, and geometric properties that determine ground-penetrating radar performance *Proc. 7th Int. Conf. on Ground Penetrating Radar (Lawrence, Kansas, 27–30 May)* pp 177–82

Pérez-Gracia V 2001 Evaluación GPR para aplicaciones en arqueología y en patrimonio histórico-artístico *PhD Thesis* Catalonia Polithecnic(UPC), Barcelona, Spain (in Spanish)

Pérez-Gracia V, García García F and Rodriguez Abad I 2008a GPR evaluation of the damage found in the reinforced concrete base of a block of flats: a case study *NDT&E Int.* **41** 341–53

Pérez-Gracia V, Gonzàlez-Drigo R and Di Capua D 2008b Horizontal resolution in a non-destructive shallow GPR survey an experimental evaluation *NDT&E Int.* **41** 611–20

Reppert P M, Dale Morgan F and Nafi Toksöz M 2000 Dielectric constant determination using ground-penetrating radar reflection coefficients *J. Appl. Geophys.* **43** 189–97

Rial F I, Pereira M, Henrique L, Arias P and Novo A 2009 Resolution of GPR bowtie antennas: an experimental approach *J. Appl. Geophys.* **67** 367–73

Salih S A 2006 Applications of ground penetrating radar (GPR) in detection of groundwater table. GORS *Proc. 15th Int. Symp. and Exhibition on Remote Sensing and Assisting Systems at General Organization of Remote Sensing Damascus (Syria, 18–21 September)*

Sandmeier K J 2011 Reflexw 6.0 manual Sandmeier Software, Zipser Strabe1, Karlsruhe, Germany

Sharma P V 1997 *Environmental and Engineering Geophysics* (Cambridge: Cambridge University Press) pp 310–28

Shaw M R, Millard S G, Molyneaux T C K, Taylor M J and Bungey J H 2005 Location of steel reinforcement in concrete using ground penetrating radar and neural networks *NDT&E Int.* **38** 203–12

Sun J and Young R A 1995 Recognizing surface scattering in ground-penetrating radar data *Geophysics* **60** 1378–85

Taner M T and Koehler F 1969 Velocity spectra–digital computer derivation and applications of velocity functions *Geophysics* **34** 859–81

Van der Kruk J and Slob E C 2004 Reduction of reflections from above surface objects in GPR data *J. Appl. Geophys.* **55** 271–8

Yilmaz O 1987 *Seismic Data Processing* ed B E Neitzel (Tulsa, OK: Society of Exploration Geophysicists) pp 166–82